MR Imaging of the Orbital Apex:

Anatomy and Pathology[1]

Ho Kyu Lee, M.D., Chang Jin Kim, M.D.[2], Hyosook Ahn, M.D.[3], Ji Hoon Shin, M.D., Choong Gon Choi, M.D., Dae Chul Suh, M.D.

The apex of the orbit is basically formed by the optic canal, the superior orbital fissure, and their contents. Space-occupying lesions in this area can result in clinical deficits caused by compression of the optic nerve or extraocular muscles. Even vascular changes in the cavernous sinus can produce a direct mass effect and affect the orbit apex. When pathologic changes in this region is suspected, contrast-enhanced MR imaging with fat saturation is very useful.

According to the anatomic regions from which the lesions arise, they can be classified as belonging to one of five groups; lesions of the optic nerve-sheath complex, of the conal and intraconal spaces, of the extraconal space and bony orbit, of the cavernous sinus or diffuse. The characteristic MR findings of various orbital lesions will be described in this paper.

The apex of the orbit is a complex region which contains many nerves, vessels, soft tissues, and bony structures such as the superior orbital fissure and the optic canal (1-3), and is likely to be involved in various diseases (3). On the basis of the anatomic components involved, pathology of the orbital apex can be classified as lesions of the optic nerve sheath complex, of the conal and intraconal spaces, of the extraconal space and bony orbit, of the cavernous sinus, and diffuse. The purpose of this paper is to review the normal anatomy of the orbital apex, as seen on MR images, and to demonstrate the wide spectrum of pathology involving this region.

Anatomy of the orbital apex

The orbital apex region consists of the optic nerve-sheath complex, the conal, intraconal and extraconal spaces, the bony orbit, and the cavernous sinus. The optic nerve-sheath complex consists of the optic nerve and three layers of the meninges (3). The cone or conal space is composed of the four rectus muscles and thin intermuscular membranes which join them, and extends posteriorly to the insertion of the muscle tendons on the annulus of Zinn at the orbital apex (4). The intraconal space contains orbital fat, the ophthalmic artery, cranial nerves III and VI, and the nasociliary nerve of V1. The extraconal space and bony orbit consist of the osseous orbital apex, the superior orbital fissure, and extraconal orbital fat. The bony orbit at the apex has four walls and bony canals including the optic canal and superior and inferior orbital fissures. The optic canal forms an angle of about 45 degrees with the sagittal plane of the head, tapers slightly anteriorly, and is bounded medially by

the body of the sphenoid bone, superiorly by the superior root of the lesser wing of the sphenoid bone, inferolaterally by the optic strut, and laterally by the anterior clinoid process. It contains the optic nerve and ophthalmic artery. The superior orbital fissure is a gap between the greater and lesser wings of the sphenoid bone, and cranial nerves III, IV, V1 and VI and the superior ophthalmic vein pass through it. The foramen rotundum, which contains cranial nerve V2 is just inferior and posterior to the superior orbital fissure (1, 5, 6). The inferior orbital fissure contains branches of the maxillary artery and the cranial nerve V2, which exits from the inferior aspect of the cavernous sinus and extends into the upper part of the pterygopalatine fossa through the foramen rotundum. The cavernous sinus contains the ophthalmic artery, and cranial nerves III, IV, V1, V2, and VI. It is connected to the ophthalmic vein and inferior petrosal sinus.

Orbital MR images can be obtained using a standard or surface coil. Imaging sequences include axial T1-weighted, and contrast-enhanced axial and coronal T1-weighted, with fat suppression. Coronal T2-weighted images through the optic nerve can be added as necessary for the evaluation of the optic nerve, and with adequate MR sequences, individual cranial nerves can be identified in the region of the cavernous sinus. The delineation of the cranial nerves is optimal when dynamic sequences are acquired about 30 seconds after the administration of contrast material (3).

Lesions of the orbital apex is more easily identified by means of coronal images than by axial. Coronal T1-weighted images, obtained just anterior to the optic canal, clearly demonstrate the optic nerve. Cranial nerves III, IV, and VI show low signal intensity lateral to the optic nerve within the hyperintense orbital fat, but it is not possible to distinguish them. The ophthalmic artery and veins are frequently demonstrated (Fig. 1). Axial images obtained through the optic canal reveal the optic nerve. In the superior orbital fissure, the annulus of Zinn and adjacent muscles can be seen within the hyperintense orbital fat. The anterior clinoid processes are symmetric, but may display variable signal intensities, depending on the amount of fatty marrow. The optic canals are located medial to each anterior process and lateral to the ethmoid sinuses (Fig. 2). Parasagittal images obtained through the orbital apex demonstrate the optic canal containing the optic nerve, and superior to this, the superior orbital fissure. Individual nerves in this latter region are difficult to differentiate, though the optic nerve can be identified just anterior to the anterior clinoid process. In order to demonstrate the long segment of this nerve, oblique sagittal images parallel to the long axis of the optic nerve can be added (Fig. 3). The optic canal and extraocular muscles can be clearly seen around the optic nerve at the orbital apex.

Pathology

Lesions of the optic nerve-sheath complex

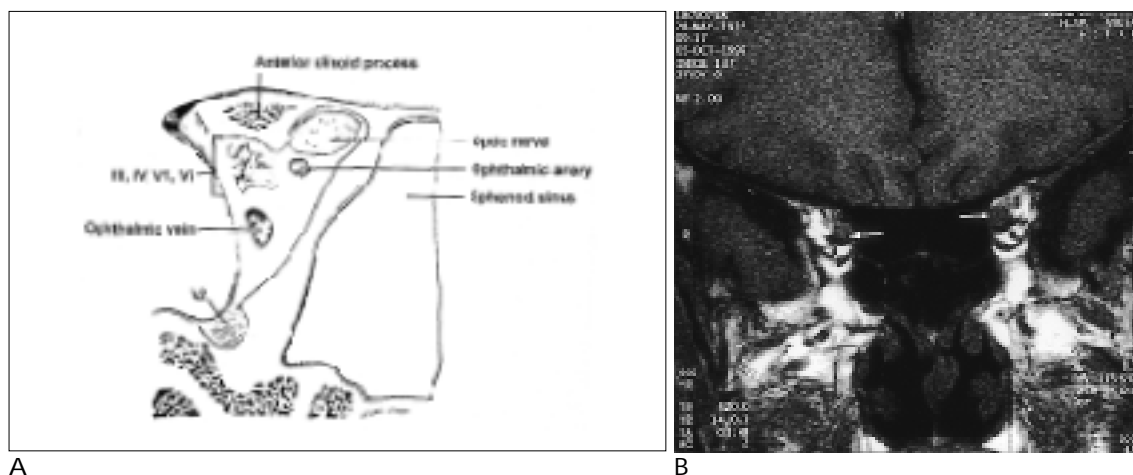These lesions are located in the central portion of the

Fig. 1. A. Schematic drawing of coronal anatomy of the orbital apex. The optic nerve and ophthalmic artery pass through the optic canal. Cranial nerves III, IV, V1 and VI and the superior ophthalmic vein pass through the superior orbital fissure. Cranial nerve V2 passes through the foramen rotundum into the inferior orbital fissure.
B. Coronal T1-weighted image of the orbital apex. Optic nerves(arrows) in the hyperintense orbital fat can be easily defined, but other cranial nerves and vascular structures are difficult to differentiate with each other.

orbital apex, and include optic nerve gliomas, perioptic meningioma, and optic neuritis. Optic nerve glioma (Fig. 4) is an uncommon, low grade neoplasm that can involve various portions of the retrobulbar visual pathway, including the optic nerve, optic chiasm, optic tract and optic radiation. Fifteen percent or more of patients with optic nerve glioma demonstrate findings of neurofibromatosis type 1 at the time of diagnosis (4), and the incidence of this condition in patients with this type of neurofibromatosis can be as high as 50%. The involvement of both optic nerves invariably indicates underlying neurofibromatosis. The tumors usually become manifest during the first decade of life, showing enlargement of the nerve, and kinking and buckling appearance are characteristic features. Menigiomas (Fig. 5) account for 5-7% of all primary orbital tumors (3). Middle-aged women are most frequently affected, but the condition also occurs in children and adolescents in association with neurofibromatosis type 1. In perioptic meningioma the so-called" tram track sign", caused by fusiform enhancement of a circumferential tumor is seen. Optic neuritis most frequently presents as a manifestation of multiple sclerosis. To detect the abnormal signal intensity of the optic nerve, the SPIR-FLAIR sequence, consisting of both the SPIR(selective partial inversion recovery) pulse for fat suppression and the FLAIR(fluid attenuated inversion recovery) sequence for water suppression, is most sensitive (7).

Conal and intraconal lesions

The cone is formed by the four rectus muscles and their connecting septa. Conal and intraconal lesions
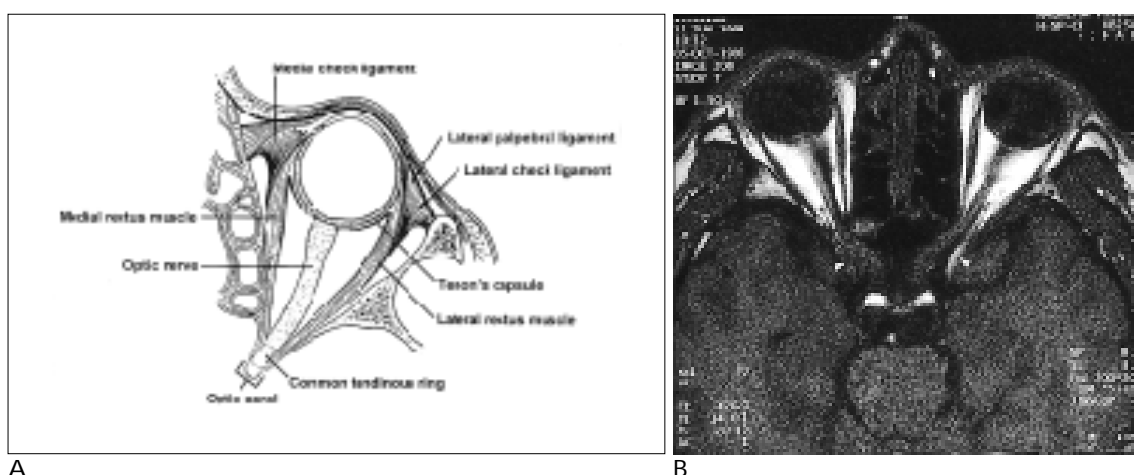

Fig. 2. A. Schematic drawing of transverse anatomy of the orbital apex through the optic canal.
B. Axial T1-weighted image of the orbital apex through the optic canal. Optic nerves in the optic canals approximately make a right angle each other. Anterior clinoid processes(arrow heads) are located just lateral to the optic nerves.
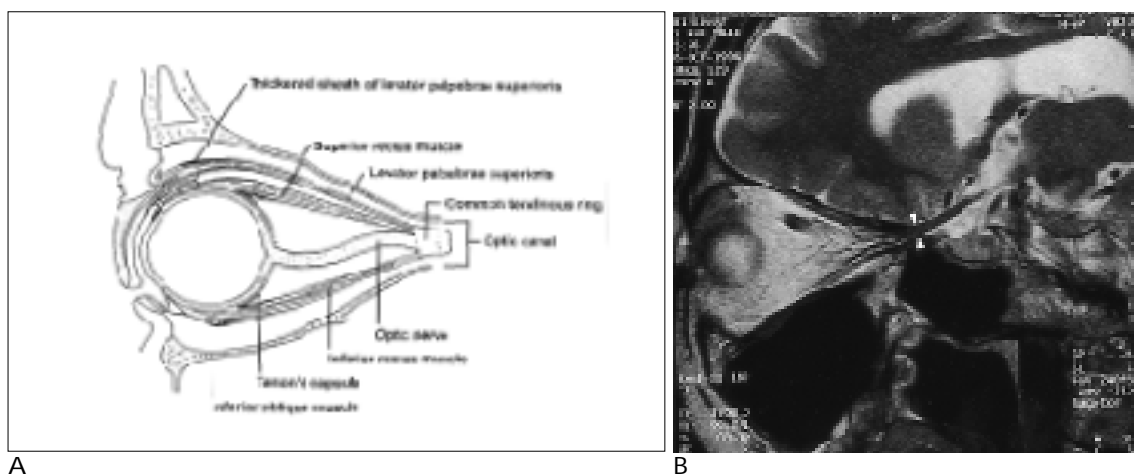

Fig. 3. A. Schematic drawing of sagittal anatomy of the orbital apex through the orbital canal.
B. Oblique sagittal T2-weighted image through the optic canal(arrow heads) shows the long course of the optic nerve.

comprise hemangioma, lymphoma, pseudotumor, lymphangioma, varix, carotid-caverous fistula, and nerve-sheath tumor. In the adult, orbital hemangioma (Fig. 6) is the most common neoplasm of the orbit. Hemangioma is classified as cavernous or capillary, the former type being more common than the latter. The condition is usually intraconal but may also extend into the extraconal space. Generally, cavernous hemangioma molds itself to pre-existing structures without causing bone erosion or enlarging the orbit. MR imaging reveals an isointense or mixed signal on T1-weighted images, and one which is hyperintense or isointense on T2-weighted images. Capillary hemangioma, also known as infantile hemangioma, is an uncommon vascular tumor, and is usually seen during the first year of life. Rapid growth during the first 6-10 months is very common, and is usually followed by spontaneous involution during preschool years. Although capillary hemangioma is most commonly extraconal, it sometimes involves the intraconal space (1). Hemorrhage or vascular structures are sometimes noted within the tumor. Schwannoma accounts for 1-6 % of all orbital neoplasms which present as a tumor in the conal or intraconal space, and may occur in association with neurofibromatosis 2. Schwannoma arises from cranial nerves III, IV, V and VI, sympathetic and parasympathetic fibers, and the ciliary ganglion. It is a well-encapsulated tumor and may be associated with hemorrhaging and cystic change (1, 4). Orbital lymphoma tends to involve the intraconal space. MRI usually reveals a hypointense lesion on both T1- and T2-weighted images. The hypointensity, seen on T2-weighted images is thought to be secondary to the highly cellular nature of the neoplasm and may help differentiate lymphoma from other diseases (4).
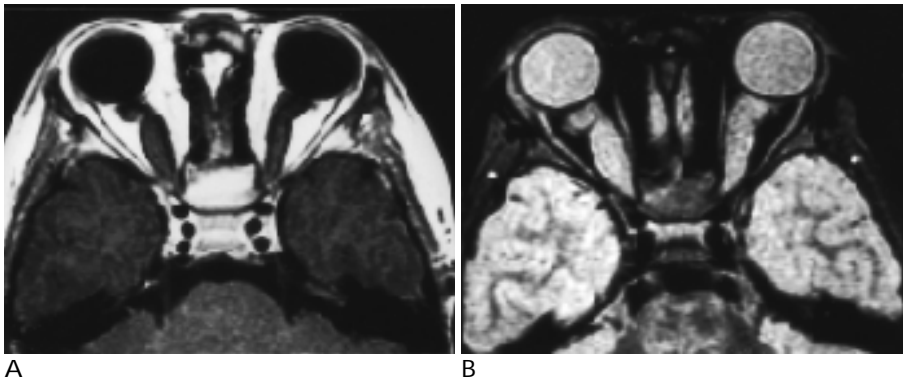

A   B

Fig. 4. Optic nerve glioma in association with neurofibromatosis type I.
A. Contrast-enhanced T1-weighted image shows diffuse enlargement of both optic nerves with subtle enhancement of the tumors. Involvement of both optic nerves invariably indicates underlying neurofibromatosis.
B. Short time inversion recovery MR image well shows characteristic kinking and buckling appearance of the tumor.
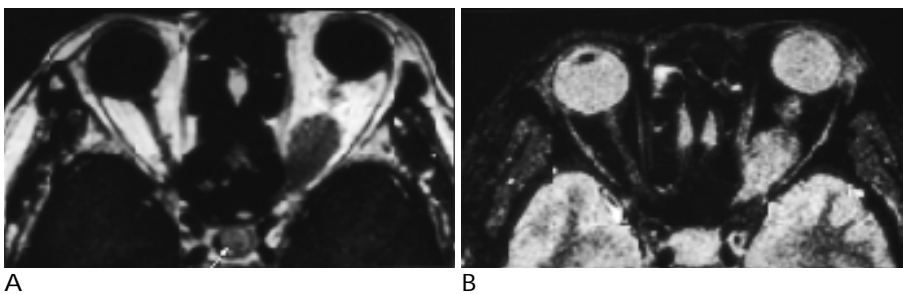

A   B

Fig. 5. Optic nerve sheath meningioma.
A. Axial T1-weighted image shows fusiform enlargement of the optic nerve sheath complex with intracranial extension, which has a mild enhancement (arrow).
B. Short time inversion recovery MR image well shows a fusiform solid tumor, but on this image the optic nerve is not discernible from the tumor.
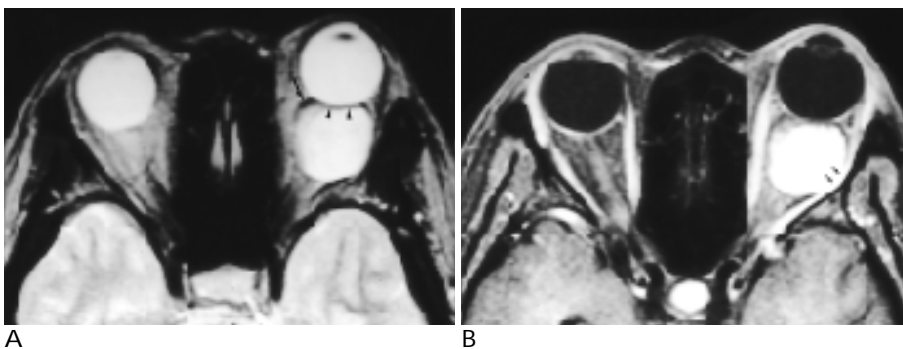

A   B

Fig. 6. Cavernous hemangioma.
A. Axi-al proton density weighted image shows a round intraconal tumor which molds itself to the eyeball(arrow heads). The dark rim of the tumor is caused by a chemical shift artifact(arrow).
B. Con-trast-enhanced T1-weighted image with fat saturation shows strong enhancement of the tumor displacing the lateral rectus muscle(arrows).
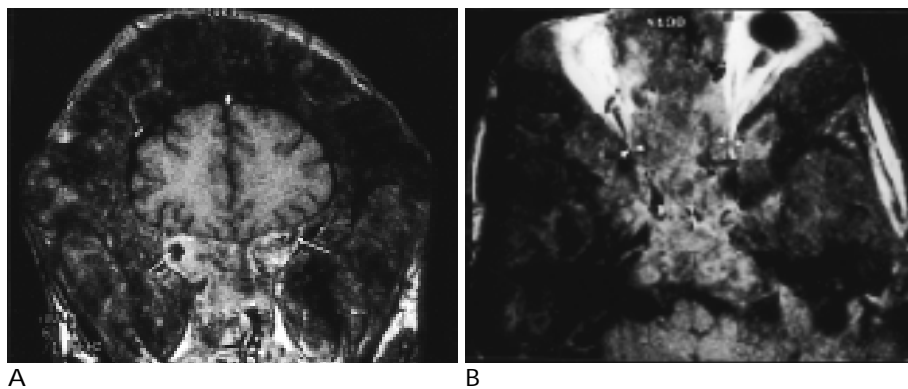
Lesions in the extraconal space and bony orbit

The extraconal space is found between the muscular cone and bony orbit. Lesions in this space are uncommon and include lymphoma, dermoid/epidermoid, hemangioma, or nerve sheath tumor. In contrast, lesions of the bony orbit are more common and include fibrous dysplasia, metastasis, Langerhans cell histiocytosis, and Paget's disease. Fibrous dysplasia (Fig. 7), which is the most common benign condition involving the bony orbit, is a developmental abnormality of the bone characterized by the abnormal growth of the fibroblasts and abnormal mineralization. Depending on the fibrous and osteoid matrix, the appearance of the medullary space shows variety between lucency and dense calcification, and there may be associated hemmorrhaging or cystic change (1, 4). MR images show low to intermediate signal intensities at all pulse sequences, and usually demonstrate intense contrast enhancement. Hematogenous bone metastasis is the most common malignant neoplasm involving the bony orbital apex. In adults, a primary tumor usually arises from the lung, kidney, breast, or prostate. In children, the most common metastatic tumors are embryonal tumors, neuroblastomas (Fig. 8) and Ewing's sarcoma (8). A metastatic bone tumor usually shows osteolytic change, but occasionally causes bone expansion especially in cases of thyroid or renal cancer (1). MR images show replacement of normal bone marrow and loss of high signal intensity on both T1- and T2-weighted images, and lesion enhancement after the injection of contrast material is also usually seen.

Lesions of the cavernous sinus

Lesions of the cavernous sinus are various and include metastasis, skull base tumor, inflammation, vascular lesion, and nerve sheath tumor. Metastasis is the most common malignant neoplasm involving the cavernous sinus. In addition to metastases to the osseous sellar region, metastatic deposits in the cavernous sinus can damage the innervation of the extraocular muscles and result in the ocular motility disturbance. The most frequent metastatic tumor that follows this pattern is breast cancer (2). Nasopharyngeal carcinoma (Fig. 9) can involve any portion of the skull base. The tumor spreads through the foramen lacerum and petro-occipital fissure along the lateral aspects of the sphenoid body and can reach the cavernous sinus and middle cranial fossa. Lateral extension of the tumor can reach the cavernous sinus through the foramen ovale. Nasopharyngeal carcinoma can selectively follow a nerve or its sheath. The

A   B

Fig. 7. McCune-Albright syndrome which consists of polyostotic fibrous dysplasia and endocrine dysfunction.
A. Contrast-enhanced coronal T1-weighted image shows polyostotic fibrous dysplasia with macrocephaly, which produces marked thickening of calvarium and facial bones. Signal void structures are dilated superior ophthalmic veins(arrows).
B. Axial T1-weighted image shows diffuse involvement of the skull base with the severe encroachment of the orbital apices(arrow heads). This patient also has a growth hormone producing pituitary adenoma.
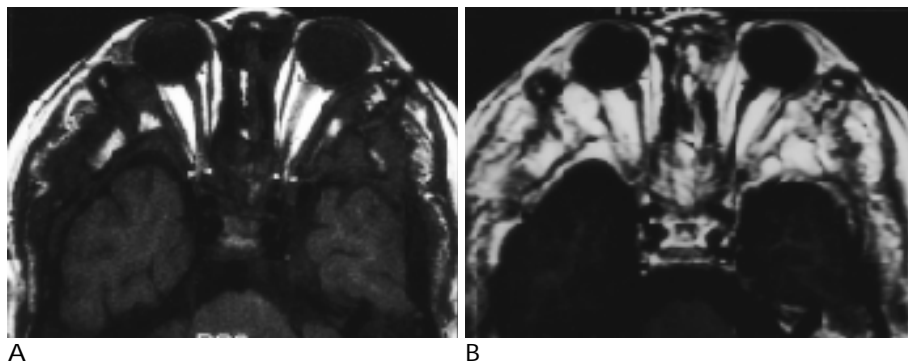
A   B

Fig. 8. Secondary neuroblastoma involving the calvarium.
A. Axial T1-weighted image shows diffuse thickening of the calvarium including both orbits. Therefore, it produces shrinkage of orbital apices(arrow heads).
B. Con-trast-enhanced T1-weighted image shows significant enhancement of the calvarial lesion.

most well-known perineural tumoral pathway to and through the central skull base is via the cranial nerve V3 (1). Tolosa-Hunt syndrome, as a variant of pseudotumor, consists of painful ophthalmoplegia, with a rather benign course and good responsiveness to corticosteroids. Histologic descriptions attribute the cause of this syndrome to granulation tissue in the cavernous sinus at the orbital apex along the superior orbital fissure (1). Fibrosing Inflammatory pseudotumor of the skull base, as one variant of pseudotumor, shows hypointensity on T2-weighted images, explained by diffuse fibrotic change with collagen deposition, but is not confined to the cavernous sinus, and usually extends to the dura, skull base, orbit and infratemporal fossa (9). Thrombophlebitis of the cavernous sinus (Fig. 10) can be caused by paranasal sinusitis, sometimes with extension to the superior ophthalmic vein (4). Traumatic carotid cavernous fistula (Fig. 11) and dural arteriovenous fistula produce protosis, enlargement of the extraocular muscles, and engorgement of the superior ophthalmic vein
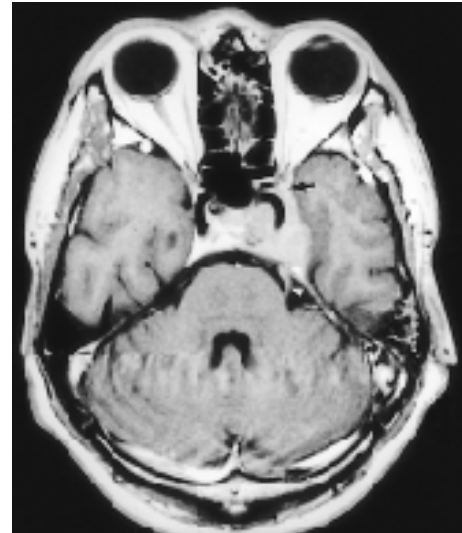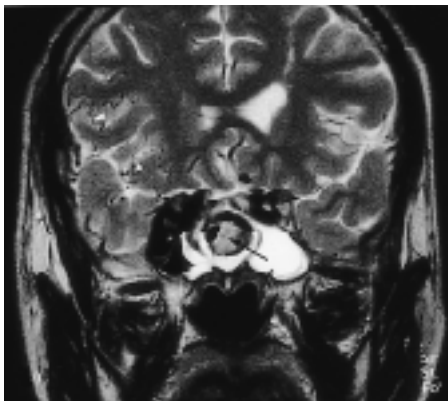

Fig. 9. Metastasis into the cavernous sinus from nasopharyngeal carcinoma. Contrast-enhanced T1-weighted image demonstrates bulging mass in the left cavernous sinus with extension to the anterior cavernous sinus(arrow). The tumor also has a perineural extension through the trigeminal nerve(arrow head).
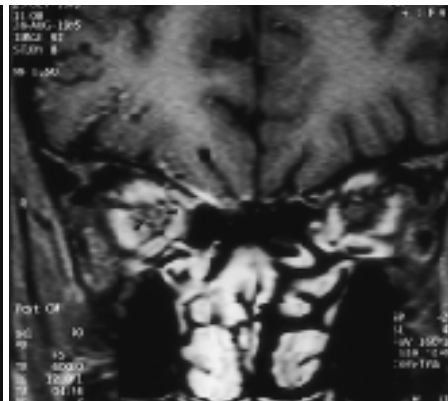

A   B

Fig. 10. Traumatic carotid-cavernous fistula.
A. Coronal T2-weighted image shows dilated vascular structures having signal voids in the right cavernous sinus with a pseudoaneurysm(arrow) in the sphenoid sinus. Numerous cortical vasculatures(white arrow heads) suggesting cortical venous drainage are demonstrated on the right cerebral hemisphere.
B. Contrast-enhanced coronal T1-weighted image with fat saturation shows swelling of extraocular muscles on the right and circumferential enhancement around the optic nerve(black arrow heads) suggesting venous engorgement of the optic nerve sheath, which are caused by increased venous pressure.
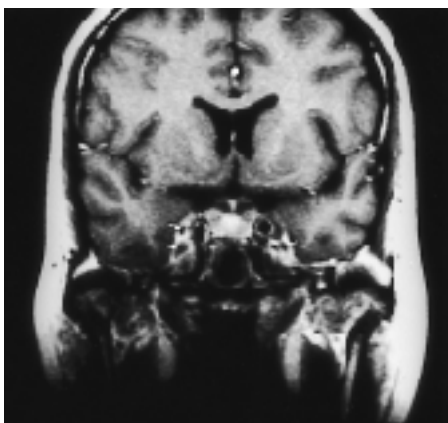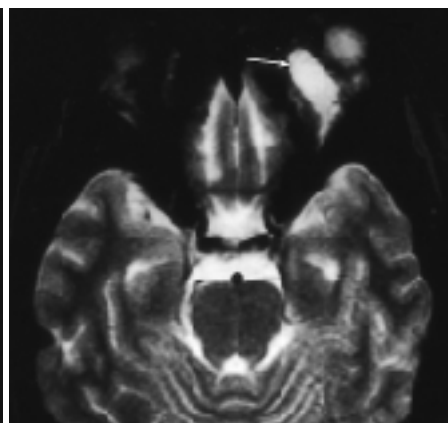

A   B

Fig. 11. Thrombophlebitis of the cavernous sinus.
A. Contrast-enhanced coronal T1-weighted image shows swelling of both the cavernous sinuses and multiple filling defects(arrows) within it, suggest of thrombosis.
B. Axial T2-weighted image shows associated thrombosis of the superior ophthalmic vein(arrow).
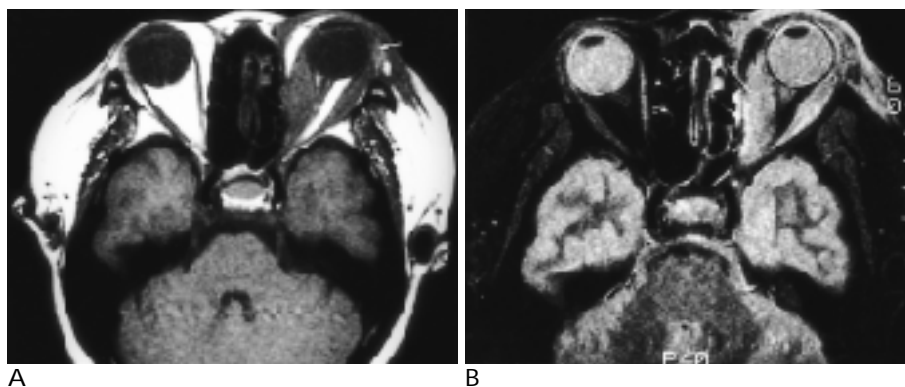
Fig. 12. Pseudotumor of the orbit.
A. Axial T1-weighted image shows diffuse involvement of the extraocular muscles and eyelid region including the lacri-mal gland(arrow).
B. Short time inversion recovery MR image well demonstrates diffuse involvement of the orbit, especially medial rectus muscle(arrow).
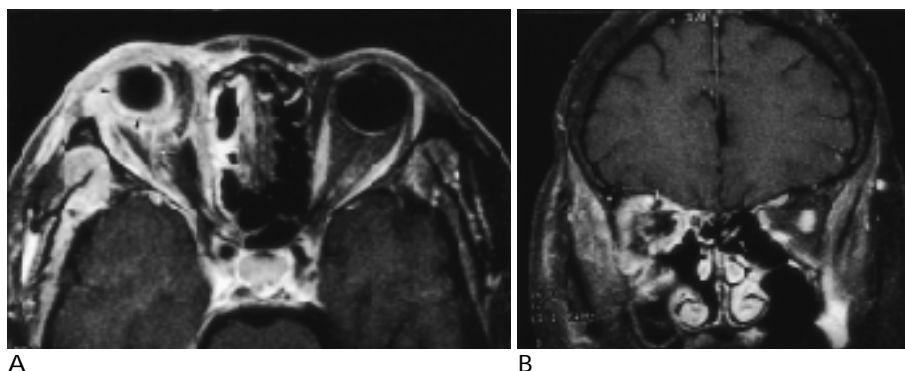
Fig. 13. Orbital cellulitis with scleritis.
A. Contrast-enhanced axial T1-weighted image with fat saturation shows diffuse enhancement of orbital soft tissue, eyelid, and temporalis muscle. Shrinkage of the eyeball with thick sclera(arrow heads) means scleritis. Thrombosis of the superior ophthalmic vein(arrow) is associated.
B. Contrast-enhanced coronal T1-weighted image shows orbital inflammation with pus collection in the superior rectus muscle complex(arrow).

(1). MR images show enlargement of the cavernous sinus, thickening of the extraocular muscles and dilatation of the superior ophthalmic vein. In cases of dural arteriovenous fistula of the cavernous sinus, contrast-enhanced T1-weighted images can show heterogeneous signal intensities within this sinus. In order to detect perineural tumor extension, contrast-enhanced T1-weighted imaging is also mandatory.

Diffuse lesions

Diffuse lesions of the orbital apex are those that involve two or more orbital spaces, and include lymphoma, pseudotumor, inflammation, and varix. Orbital pseudotumor (Fig. 12) is similar in many respects to orbital infection, but with greater severity of the signs and symptoms. Even a mass lesion does not usually invade or distort the shape of the globe. Both clinically and radiologically, it is very difficult to differentiate between pseudotumor and lymphoma (1). Orbital pseudotumor shows intermediate to high signal intensity on T2-weighted images, and dense enhancement after the injection of contrast material is also usually seen. Orbital infection (Fig. 13) can involve the orbital apex, and is most frequently caused by paranasal sinusitis. The involved orbit shows inflammatory edema, subperiosteal abscess, orbital cellulitis, orbital abscess, and thrombosis of the ophthalmic vein and cavernous sinus. Another important and more complicated orbital infectious process results from the extension of mycotic sinonasal infection into the orbit. The most important fungal rhinocerebral infections are aspergillosis and mucormycosis (1). Because paramagnetic substances are present in the fungus ball, MR images may show low signal intensities at all pulse sequences. Vascular thrombosis and ischemic or hemorrhagic brain infarction caused by invasion of the cerebral blood vessels due to fungal infection can also be demonstrated on MR images, especially in cases of mucormycosis.

Conclusion

On the basis of the anatomic components from which lesions of the orbital apex originate, these were categorized as belonging to one of five groups. For the differential diagnosis of various orbital apex lesions, this approach is useful, and we believe that contrast-enhanced T1-weighted MR imaging with fat saturation is the pulse sequence which most effectively demonstrates various pathologies involving the orbital apex.

References

1. Mafee MF. *Eye and orbit.* In: Som PM, Curtin HD. *Head and neck imaging.* 2nd ed. St. Louis: Mosby, 1996:1059-1128
2. Daniel DL, Yu S, Pech P, Haughton V. CT and MRI of the orbital apex. *Radiol Clin North Am* 1987;25:803-817
3. Hosten N, Bornfeld N. *Imaging of the globe and orbit: a guide to differential diagnosis.* Stuttgart: Thieme, 1998:126-132
4. Koeller KK. Smirniotopoulos JG. Orbital masses. *Semin Ultrasound CT MR* 1998;19:272-291
5. Daniel DL, Pech P, Kay MC, et al. Orbital apex: correlative anato-mic and CT study. *AJNR* 1985; 6:705-710
6. Daniel DL, Mark L, Mafee MF, et al. Osseous anatomy of the orbital apex. *AJNR* 1995;16:1929-1935
7. Jackson A, Sheppard S, Laitt RD, Kassner A, Moriarty D. Optic neuritis: MR imaging with combined fat- and water-suppression technique *Radiology* 1998;206:57-63
8. Bilaniuk LT, Atlas SW, Zimmerman RA. *The orbit.* In: Lee SH, Rao KCVG, Zimmerman RA. *Cranial MRI and CT.* 3rd ed. New York: McGraw-Hill, 1992:119-192
9. Han MH, Chi JG, Kim MS, er al. Fibrosing inflammatory pseudo-tumors involving the skull base: MR and CT manifestations with histopathologic comparison. *AJNR* 1996;17:515-21

MR : [1]

[1] , [2] , [3]

. [2] [3] . .

,

.

.

.

MR

, , ,

, , 5

.